Vitrification of municipal solid waste incineration fly ash: An approach to find the successful batch compositions

Availability:
This version is available at: 11583/2874967 since: 2021-03-17T17:38:15Z

Terms of use:

This article is made available under terms and conditions as specified in the corresponding bibliographic description in the repository

(Article begins on next page)

20 April 2024

Vitrification of municipal solid waste incineration fly ash: an approach to find the successful batch compositions

Elham Sharifikolouei[1,*], Francesco Baino[1], Milena Salvo[1], Tonia Tommasi[2], Raffaele Pirone[2], Debora Fino[2], Monica Ferraris[1]

Institute of Materials Physics and Engineering, Department of Applied Science and Technology, Politecnico di Torino, Torino, Italy

Institute of Chemical Engineering, Department of Applied Science and Technology, Politecnico di Torino, Torino, Italy

Abstract

Incineration is the most common way to reduce the mass and the volume of municipal solid wastes. One of the most dangerous by-products of the incineration process is fly ash that contains a considerable amount of heavy metals. Therefore, its treatment is crucial to prevent the leaching of heavy metals into the environment. In the present work, two different sources of municipal solid waste incinerator fly ash have been vitrified in order to inhibit the release of potentially toxic heavy metals. Two different sources of silica, i.e. silica sand and glass cullet, have been added to each type of fly ash in an attempt to obtain vitrifiable batches. The standard leaching test on vitrified products was performed according to EN12457-2 confirming no heavy metal leaching and, therefore, they all pass waste acceptance criteria to be classified as an inert material. Furthermore, the previously reported data for vitrification of fly ash was combined with the present work and their compositions were presented in the SiO_2-Al_2O_3-CaO, and SiO_2-ΣM_2O_3-$\Sigma(MO+M_2O)$ ternary phase diagrams to identify the region in which successful compositions are concentrated. This analysis could facilitate the attempt to find the right composition for vitrification of fly ash.

Keywords: vitrification; circular economy; municipal solid waste incinerator (MSWI); fly ash; ion leaching; waste management

1. Introduction

Following the general increase of population and industrial development, the production of municipal

---

*Corresponding author: juergen.eckert@unileoben.ac.at

solid waste in the world is expected to increase by 60% from 1.3 billion tons in 2015 to 2.2 billion tons in 2025 [1]. One of the most common ways to reduce the mass and volume of municipal solid waste while recovering its energy is the incineration process [2,3]. The most common by-products of incineration are bottom ash and fly ash which are often classified as hazardous waste materials based on their heavy metal leaching [4]. In particular, fly ash contains a significant concentration of toxic heavy metals such as mercury, lead, arsenic, chromium, as well as organic pollutants such as dioxins. There is a large body of research going on to propose proper treatment for fly ash such as their incorporation in the cement structure, sintering methods, wet chemical treatments, and vitrification [5–8]. Most of these techniques are challenging because the high amount of chlorides in the fly ash is a critical issue, especially for cement-based techniques [9,10]. Vitrification is a very promising process for the safe treatment of hazardous ash and suppression of heavy metal leaching; even radioactive waste, which belongs to the most hazardous class of waste, can be successfully treated by vitrification [11,12]. While bottom ash may be directly vitrified as such [13,14], direct vitrification of fly ash is often challenging since they contain a limited amount of glass-forming oxides such as SiO_2. Some researchers have tried to vitrify fly ash directly through plasma treatment at high temperature (1600˚C). Bernardo et al [15] have utilized plasma treatment to produce leach-resistance glass from municipal solid waste. However, plasma treatment is a high-energy consumption solution. Bernardo et al. have argued that such energy consumption could be less in some countries such as France because of its infrastructure for plasma treatment of wastes. Similarly, other researchers [16,17] have used a plasma torch to directly vitrify fly ash. The fly ash composition they have used contain between 32 wt% to 58 wt% SiO_2 which is not quite common for municipal solid waste incinerators fly ash. Furthermore, the high temperature treatment raises concern about vaporization of toxic elements into the atmosphere. Yan et al has reported a considerable weight loss after plasma treatment, which might be accountable for vaporization of heavy elements and dioxin. To reduce the treatment temperature, many researchers have attempted to prepare a fly ash vitrification batch through the addition of additives. Alhadj-Mallah et al [18] decreased the plasma treatment temperature of fly ash with 58 wt% SiO_2 down to 1300˚C through the addition of biomass ash to the batch. The aim of vitrification is not always focused on the final amorphous structure, and it may be focused on the heavy metal leaching behavior of vitrified products. Vu et al [19] has used the mixture of bottom ash and fly ash to produce glass-ceramics with acceptable leaching resistance with bottom ash: fly ash ratios of 90:10, 80:20, 60:40, and 50:50 at 950˚C. The other common way to vitrify fly ash is through the addition of glass-forming additives such as glass cullet or silica sands; the melting temperature varies a lot depending on

the fly ash composition and is reported to be in the range of 1100°C to 1500°C [18,20]. The objective is to encapsulate the hazardous elements within the glass matrix, making them less susceptible to leaching or chemical attacks [21].

Fly ash compositions differ a lot depending on the region and the technology of the incinerator; therefore, a systematic study is required to identify the compositional regions in the phase diagram of main oxides where fly ash can be vitrified. Recently, Gao et al have shown that the addition of fluxing agents, such as B_2O_3, allows decreasing the fly ash melting point to about 990°C (with the addition of 15 wt% B_2O_3) [22]. The addition of B_2O_3 as a fluxing agent in large scale vitrification of fly ash could introduce new costs and consequently, processes that do not require fluxing agents are preferred. Therefore, in the present work, the vitrification has been promoted by the addition of silica sand and glass cullet as a source of SiO_2. Furthermore, we have tried to identify the compositional ranges for the fly ash vitrification in the ternary phase diagram of the main three oxides in the batch: SiO_2-Al_2O_3-CaO, as well as the SiO_2-ΣM_2O_3-$\Sigma(MO+M_2O)$ ternary phase diagram. We have shown, in all successfully vitrified fly ash batches, the specific range of values for CaO/SiO_2 molar ratios; furthermore, the number of non-bridging oxygens per tetrahedron (NBO/T) is reported. Since some scientists prefer to work directly with the degree of polymerization in the oxide melt, such correlation is also presented for the factor Q (Q=4-NBO/T). Finally, the leaching behavior of the successfully vitrified fly ash samples has been investigated according to the standard EN12457-2.

2. Materials and Methods

2.1   Starting Materials

Fly ash was collected from two different municipal solid waste incinerators: fly ash no. 1 (FA1) was collected from a waste-to-energy plant with grid furnace technology while fly ash no. 2 (FA2) was collected from an incinerator with fluidizing bed technology. Vitrification batches were prepared by the addition of glass cullet, and mine filling silica sand (S). All materials were kindly provided by Neorurale s.r.l (Italy).

The chemical analysis of FA1 and FA2 was performed by X-ray fluorescence (XRF, RIGAKU ZSX100E 68 equipped with a Rh X-ray tube and TAP, PET, LiF1, Ge, RX61 and RX45 69 analysis crystals). The mineralogical phase analysis was performed by X-ray diffraction (XRD) using Bruker D4-ENDEAVOR operating at 40 kV/30 mA with Bragg-Brentano geometry, CuKα incident radiation (wavelength λ = 0.15405 nm), step size 0.02° and fixed counting time of 1 s per step.

The leaching test was conducted following the standard EN12457-2. Briefly, FA1 and FA2 were mixed with distilled water using a solid to liquid volume ratio of 1:10, and the suspension-containing flasks were put in an orbital incubator (100 rpm) at 25°C for 24 hours. The filtered (0.2 µm mesh) solutions were analyzed by using inductively coupled plasma mass spectrometry (ICP-MS, iCAP Q, ThermoFisher) in order to detect the concentration of heavy metal ions after the leaching test.

2.2   Vitrification Process

The weight ratios of fly ash to additives (glass cullet, silica sand) in the vitrification batches is reported in Table 1. The batches were prepared in fly ash: additive ratio of 1:1 because on an industrial scale, this is the most feasible vitrification batch while providing enough Silica content on the final batch. The batches were placed in alumina crucibles (230 ml, Almath Crucible Ltd, Newmarket, UK) and were heated up to 1300°C and 1450°C for glass cullet batch and silica sand batch, respectively. The vitrification temperatures were selected based on the lowest possible temperature to cast the glass. The batches were heated with the rate of 20°C/min, and 2 hours of dwelling time. The melts were cast onto a brass plate in air.

Table 1. Mass ratios (wt%) of additives and fly ash in vitrification batches.

Batch	FA1	FA2	Silica sand	Glass cullet	Vitrification Temperature
G1	50	-	50	-	1450°C
G2	-	50	50	-	1450°C
G3	50	-	-	50	1300°C
G4	-	50	-	50	1300°C

2.3 Characterization of vitrified batches

Each batch was analyzed by XRD (under the experimental conditions already described in section 2.1) and energy dispersive spectroscopy (EDS, JCM - 6000Plus Versatile Benchtop JEOL, for compositional assessment) after vitrification followed by the leaching test according to EN12457-2. As regards the ion release tests, the vitrified products were dry ball milled in order to obtain a particle size < 4 mm, and the powders were then mixed with distilled water; the suspensions were prepared, processed and analyzed as already described in section 2.1.

3. Results and Discussion

The XRF analysis of FA1, FA2, silica sand and glass cullet are presented in Table 2. As expected, FA1 and FA2 contain a high amount of chloride and metal oxides and only approximately 14 wt% of SiO_2,

which is the glass forming oxide. In the present work, glass cullet and silica sand were therefore added to the fly ash to provide an external source of silica. It is also noticeable the presence of heavy metals, which are prone to be released from the fly ash as such, as shown later.

XRD analysis was carried out on FA1 and FA2 (Figure 1) to identify the mineral phases. Figure 1 shows that chloride salts such as halite and sylvite are the major mineralogical phases. Therefore, the alkali oxides could be written as their salts following the equation (1) and equation (2):

$$2Na_2O + 4Cl^- \rightarrow 4NaCl + O_2 \tag{1}$$

$$2K_2O + 4Cl^- \rightarrow 4KCl + O_2 \tag{2}$$

FA2 contains significantly more CaO than FA1, which has led to the emergence of the Portlandite phase. On the other hand, FA1 has Periclase as one of its main crystalline phases due to its higher amount of MgO.

Table 2. XRF analysis of FA1, FA2, Silica Sand, and Glass cullet.

| Composition (wt%)	FA1	FA1	Glass cullet	Silica sand
Na_2O	5.83	5.55	11.38	0.00
MgO	6.53	2.29	0.93	0.00
Al_2O_3	22.73	18.19	3.38	0.20
SiO_2	14.02	14.35	64.46	99.75
P2O5	0.82	1.23	0.00	0.00
Cl^-	14.82	13.72	0.00	0.00
K_2O	3.08	3.22	1.97	0.00
CaO	20.22	32.49	9.73	0.05
TiO2	0.76	0.76	0.78	0.00
Cr_2O_3	0.08	0.02	0.01	0.00
Fe_2O_3	0.56	0.62	0.15	0.00
CoO	0.00	0.00	0.00	0.00
NiO	0.00	0.00	0.00	0.00
CuO	0.00	0.58	0.00	0.00
ZnO	1.30	0.44	0.06	0.00
Br	0.04	0.10	0.00	0.00
SrO	0.02	0.06	0.00	0.00
ZrO_2	0.00	0.00	6.69	0.00
CdO	0.00	0.00	0.00	0.00
SnO_2	0.08	0.00	0.00	0.00
Sb2O3	0.08	0.04	0.00	0.00
HgO	2.40	1.99	0.00	0.00
PbO	6.61	4.37	0.45	0.00
Total	100	100	100	100
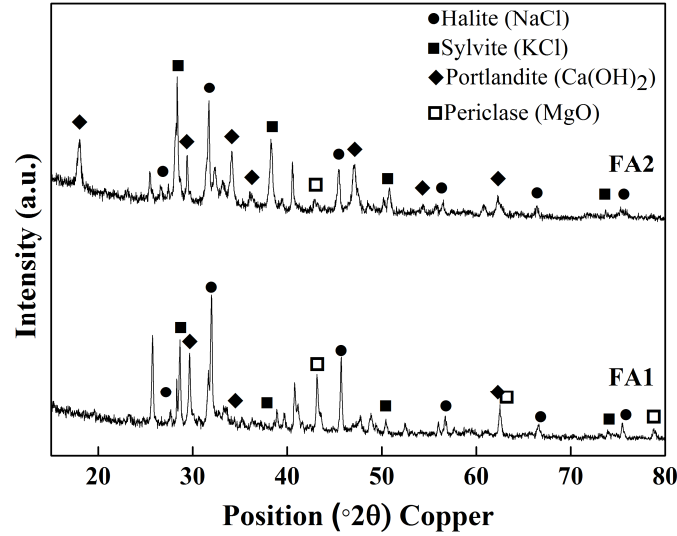
Figure 1. XRD analysis of FA1 and FA2.

Chemical composition of fly ash batches after vitrification was analyzed by EDS which is shown in Table 3. The EDS analysis shows a change of composition after the vitrification process. As observed in XRD analysis, the major mineralogical phases in FA1 and FA2 were chloride salts Halite and Sylvite. These salts are expected to evaporate at high temperatures (NaCl boiling point= 1465˚C [23], KCl boiling point = 1500˚C). The partial evaporation of these substances is a possible explanation for the reduction of Cl^-, Na_2O and K_2O, leading to higher concentration of other oxides such as CaO. However, the heavy metals such as Pb, and Hg, are still present in the batch. Therefore, vitrification is a candid process to make fly ash an inert material and to prohibit introduction of these toxic metals into the environment through landfill.

Table 3. Chemical composition of G1, G2, G3, and G4 before and after vitrification.

Composition (wt%)	G1		G2		G3		G4	
	Before	After	Before	After	Before	After	Before	After
Na_2O	2.91	2.26	2.79	1	8.5	3.99	8.39	8.82
MgO	3.26	5.41	1.15	1.36	3.71	8.63	1.6	2.23
Al_2O_3	11.45	13.47	9.25	12.9	13.01	9.45	10.81	23.58
SiO_2	56.8	54.04	57.4	53.69	38.78	43.07	39.38	43.2
P2O5	0.41	1.09	0.62	1.59	0.41	1.46	0.62	1.76
Cl^-	7.4	ND	6.9	ND	7.4	ND	6.9	0.01
K_2O	1.54	1.21	1.62	0.93	2.51	0.28	2.59	1.01
CaO	10.12	15.3	16.37	23.18	14.88	26.06	21.13	12.1
TiO2	0.38	0.94	0.38	0.57	0.76	1.35	0.76	0.67
Cr_2O_3	0.04	0	0.01	0	0.04	0	0.01	0.11
Fe_2O_3	0.28	0.86	0.31	0.75	0.35	1.8	0.38	0.65
CoO	ND	0.15	ND	ND	ND	0.3	ND	ND
NiO	ND	0.13	ND	0.04	ND	0.32	ND	ND
CuO	ND	0.09	0.29	ND	0.04	ND	0.29	0.52

ZnO	0.65	0.06	0.22	0.24	0.68	0.44	0.25	0.13
Br	0.02	2.33	0.05	2.67	0.02	2.1	0.05	3.3
SrO	0.01	ND	0.03	ND	0.01	ND	0.03	ND
ZrO_2	ND	0.82	ND	0.74	3.29	0.52	3.29	1.04
CdO	ND	0.28	ND	ND	ND	ND	ND	0.24
SnO_2	0.04	ND	ND	ND	0.04	ND	ND	ND
Sb2O3	0.04	ND	0.02	ND	0.04	ND	0.02	ND
HgO	1.20	0.47	1.00	0.32	1.20	0.21	1.00	0.56
PbO	3.30	1.09	2.20	0.03	3.50	ND	2.40	0.09
Total	100	100	100	100	100	100	100	100

ND: No Detection; Below detection limit

Because of the importance of oxide molar ratios, the main three oxides (SiO_2, CaO, Al_2O_3) molar ratios are shown in Table 4. Clearly, the addition of 50 wt% silica sand or glass cullet has increased the silica content to an acceptable range for vitrification in all batches. However, compared to the common glasses in the SiO_2-Al_2O_3-CaO system, alumina content in (G1-G4) batches is low[24]. The structure of glass is composed of Si-based and Al-based tetrahedra joined by bridging oxygen in two ways: Si-O-Si and Si-O-Al. These aluminosilicate frameworks are characterized by their degree of polymerization [25]. Since the $[AlO_4]^{5-}$ units introduce charge imbalance into the system, their structural role is more complex and depends on CaO/Al_2O_3 (C/A) molar ratio [26]. The presence of CaO is necessary for providing the charge balance so that Al_2O_3 can act as a network former. However, the excessive amount of CaO (Ca^{2+}) can depolymerize the aluminosilicate network by forming non-bridging oxygens, and therefore destabilization of the glass structure can occur. Among our batches, the highest C/A ratio belongs to G2 and G3. Therefore, the crystallization is more likely to occur in G2 and G3 batches. Furthermore, the CaO/SiO_2 (C/S) ratio affects vitrification as well. Heo et al [27], has previously investigated the effect of C/S ration (C/S= 0.65-1.02) on the crystallization behavior of the CaO-SiO_2-FetO-Al_2O_3 system and has shown that a higher C/S ratio leads to easier crystallization due to the increased fluidity of the batch. In another study by Kucharczyk et al [28], the chemical compositions of fly ash were mimicked to investigate the effect of C/S ratio (C/S= 0.07-1.54) on the crystallization behavior of fly ash and the FTIR and Raman spectroscopy analysis showed similar trends to what Heo stated earlier; higher C/S ratio has led to depolymerization of glass network and, therefore, crystallization. Following this observation, in this work, G2 and G3 with higher C/S ratios are expected to devitrified more readily. Among these 4 batches, G4 has the lowest C/S and C/A ratios, making it an ideal (theoretically) batch for vitrification. On the other hand, all these working batches (G1-G4) are between the lowest and middle values in the range reported by previous works.

Table 4. Molar ratios of CaO, SiO$_2$, and Al$_2$O$_3$ after vitrification normalized in 100%

Batches	SiO$_2$ (mole%)	Al$_2$O$_3$ (mole%)	CaO (mole%)	C/S (molar ratio)	C/A (molar ratio)
G1	68.98	10.12	20.89	0.30	2.06
G2	62.36	8.82	28.80	0.46	3.26
G3	56.28	7.27	36.43	0.64	5.01
G4	61.68	19.82	18.48	0.29	0.93

Figure 3 shows the XRD analysis of four batches (G1-G4) after vitrification. As can be seen, all the batches are mostly amorphous with some minor peaks emerged in batches G2 and G3. The peaks are identified to be wollastonite. We have previously discussed that the crystallization might occur more readily in G2 and G3 for their higher C/S and C/A ratios, and the XRD results confirm that.
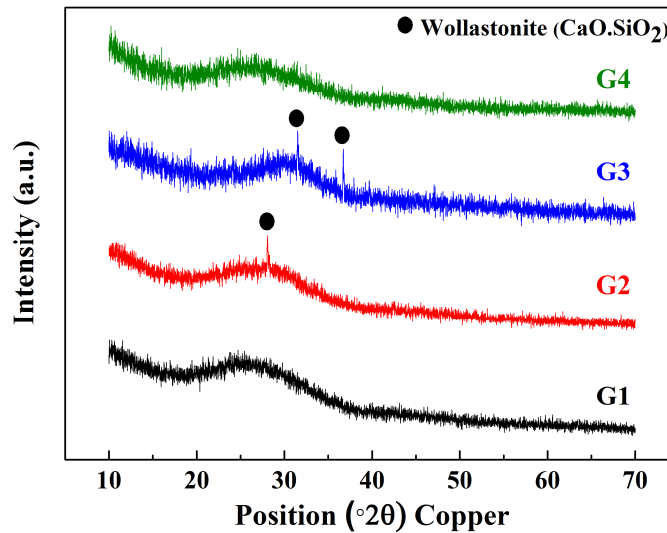

Figure 2. XRD analysis of vitrified batches

To be able to evaluate the effect of composition on vitrification of fly ash batches, our results together with previously reported successful vitrification batches are presented in the ternary phase diagrams in Figure 4. The complete list of the data-points is presented in Table 5. Figure 4-a shows the SiO$_2$-Al$_2$O$_3$-CaO ternary phase diagram in the batches in which their molar ratios are normalized, eliminating the rest of oxides to simplify the system. This way, tracking the C/S ratio for the vitrification batches is facilitated. All the reported fly ash vitrification batches have the C/S ratio in the range of 0.07 and 1.54. The distribution of C/S ratios for the batches is presented in the box chart. Clearly, 50% of the reported batches have the C/S ratio close to 0.44. this is in line with our expectation concerning the effect of the

C/S ratio on depolymerization in the glass network. Figure 4-b presents the ternary diagram for the majority of oxides in the batches reported in the literature and the present work. In this diagram, the system is divided into SiO_2, network-formers such as Al_2O_3 and Fe_2O_3 (M_2O_3), and network modifiers which are necessary for the charge balance in the glass structure such as CaO, MgO, Na_2O and K_2O (M_2O and MO). It can be observed that fly ash vitrification batches tend to be concentrated in the area marked in the circle. In order to analyze the effect of the oxides on the vitrification more quantitatively, the factor NBO/T is calculated for each batch following the equation (3)[29] where MO=CaO, MgO, $M_2O=Na_2O$, K_2O, M_2O_3= Al_2O_3, Fe_2O_3, and $MO_2=SiO_2$. NBO/T shows the degree of depolymerization in the glass and its distribution in vitrification batches is shown in the box chart. 50% of the batches have NBO/T around 0.66 and 75% of the batches have this depolymerization factor for less than 1.26.

$$\frac{NBO}{T} = \frac{2(\sum_1^{N_{MO}} X_{MO} + \sum_1^{N_{M2O}} X_{M2O} - \sum_1^{N_{M2O3}} X_{M2O3})}{(\sum_1^{N_{MO2}} X_{MO2} - 2\sum_1^{N_{M2O3}} X_{M2O3})} \tag{3}$$

Some researchers prefer to use a parameter Q to evaluate the degree of polymerization in the melt which can be calculated following the equation (4) [29,30]. We have calculated and shown the polymerization degree "Q" in the box chart. The presented data shows a high degree of polymerization for most batches, standing 75% of the data with the degree of polymerization of 3.45. However, one must pay attention to the fact that fly ash batch compositions are not completely designed for vitrification similar to classic glass batches, and the equations (3) and (4) are formulated for fully balanced systems. We know that the number of Al atoms and the charge compensators are not fully balanced in fly ash system and, therefore, this might partially explain the unusually-higher Q values.

$$Q = 4 - \frac{NBO}{T} \tag{4}$$

Table 5. Chemical composition of successfully vitrified fly ash batches.

#	SiO₂	Al₂O₃	CaO	Na₂O	K₂O	MgO	Fe₂O₃	NBO/T	Q	T	Amorphous	Ref
	%mole	%mole	%mole	%mole	%mole	%mole	%mole	-	-	˚C	-	
1	68.38	5.32	19.74	1.75	1.38	0.02	0.00	0.44	3.55	1600	Yes	[17]
2	37.07	4.09	37.00	5.01	4.29	0.02	0.01	1.74	2.25	1400	Partial	[32]
3	43.99	8.02	37.24	4.81	0.20	0.05	0.00	1.14	2.85	1600?	Yes	[15]
4	69.71	10.81	4.04	0.62	1.65	0.10	0.02	-	-	1300	Yes	[18]
5	60.24	8.84	18.27	2.46	0.86	8.98	0.35	0.54	3.46	1450	Yes	G1
6	59.66	8.45	27.59	1.09	0.66	2.25	0.31	0.59	3.41	1450	Yes	G2
7	11.41	2.04	37.78	3.97	5.88	0	0.01	4.06	0.06	1350	Yes	[33]
8	24.44	9.56	43.94	1.66	2.04	0.04	0.02	1.62	2.37	1150	Partial	[22]
9	45.74	5.92	29.65	4.11	0.19	13.67	0.72	1.38	2.61	1300	Yes	G3
10	52.17	16.77	15.65	10.31	0.78	4.02	0.29	0.32	3.68	1300	Yes	G4
11	64.58	3.98	19.78	7.63	0.55	0.03	0.00	0.66	3.33	1300	Yes	[34]

12	65.00	3.64	19.27	8.10	0.52	0.03	0.00	0.67	3.32	1300	Yes	[34]
13	65.32	3.54	18.73	8.4	0.49	0.03	0.00	0.66	3.33	1300	Yes	[34]
14	43.66	11.29	38.53	0.68	0.11	0.04	0.01	0.84	3.15	1400	Yes	[35]
15	23.80	4.95	29.32	7.79	4.74	0.06	0.01	1.84	2.15	1350	Yes	[36]
16	34.80	5.37	32.24	4.00	2.83	0.03	0.00	1.28	2.71	1500	Yes	[16]
17	35.25	4.41	22.98	4.02	3.16	0.04	0.01	0.94	3.05	1500	Yes	[16]
18	59.81	12.82	13.48	2.25	1.40	0.02	0.02	0.09	3.90	1500	Yes	[16]
19	69.63	10.76	14.79	0.17	0.93	0.00	0.03	0.11	3.88	1550	Yes	[37]
20	29.77	6.17	21.14	11.55	4.30	0.03	0	1.20	2.79	1400	Partial	[31]
21	35.98	10.74	39.84	4.54	2.16	0.04	0.02	1.24	2.75	1400	Partial	[38]
22	45.19	13.66	21.80	10.16	1.34	0.07	0.00	0.54	3.45	1500	Yes	[21]
23	55.65	10.67	16.61	9.62	1.68	0.05	0.00	0.44	3.55	1500	Yes	[21]
24	65.04	3.57	14.83	9.14	2.19	0.04	0.00	0.62	3.37	1500	Yes	[21]
25	37.35	4.64	18.02	5.32	0.47	0.33	0.00	0.83	3.16	1500	Yes	[21]
26	46.98	3.32	14.11	5.83	0.93	0.28	0.00	0.66	3.33	1500	Yes	[21]
27	53.22	2.44	11.48	6.19	1.41	0.24	0.00	0.58	3.41	1500	Yes	[21]
28	26.32	4.25	47.21	5.49	10.25	0.04	0.02	3.36	0.63	1450	Yes	[39]

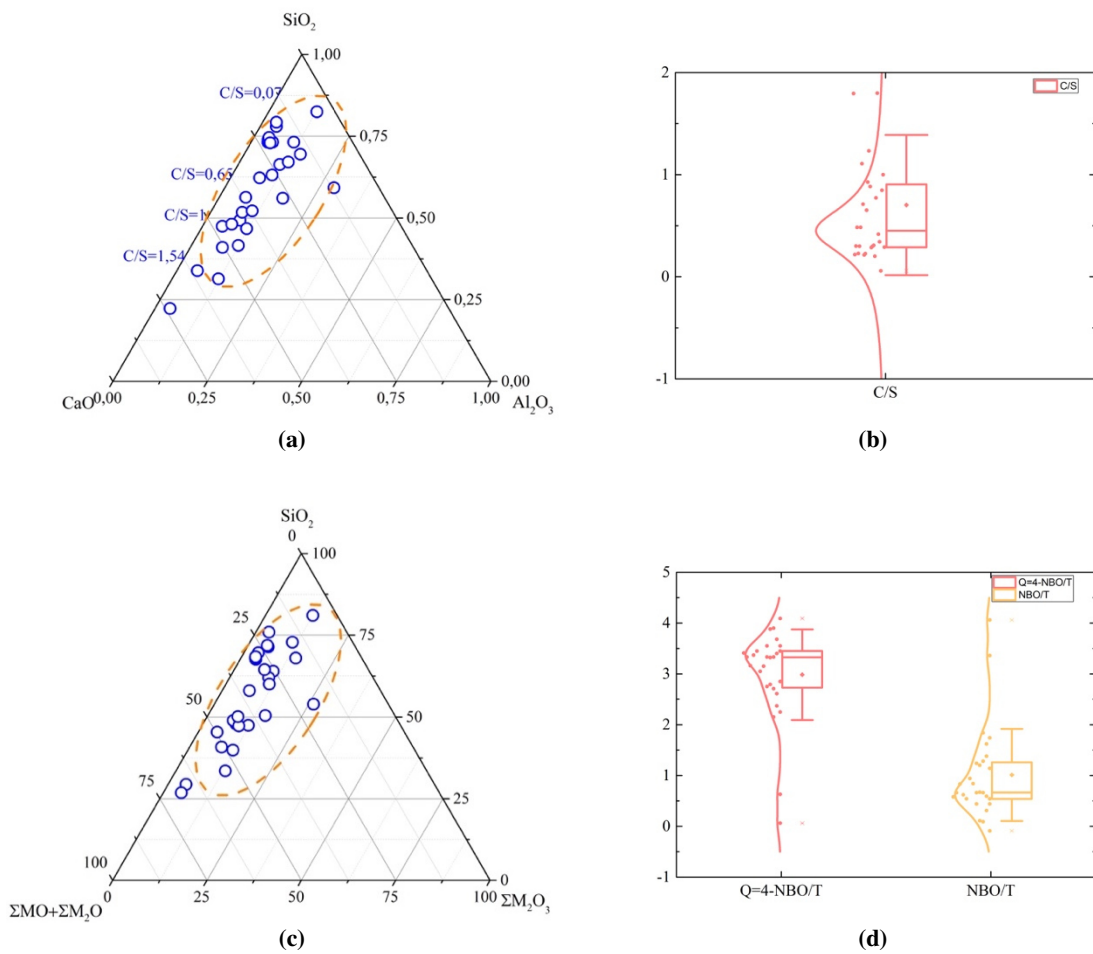*Figure 3.* (a) SiO_2-Al_2O_3-CaO phase diagram for *successful vitrification batches containing fly ash. (b) The distribution of CaO/SiO$_2$ (C/S) values for the vitrification batches. (c)* SiO_2-ΣM_2O_3-$\Sigma(MO+M_2O)$ *phase diagram for successful vitrification batches containing fly ash. (d) The distribution of NBO/T and Q for vitrification batches to present their degree of polymerization. The complete list of data points is presented in Table 5.*

To be able to evaluate if the heavy metals are safely encapsulated inside the glass structure, the leaching test was conducted on the glasses and is compared to the initial leaching test values in the fly ash (FA1, FA2) and additives (glass culet, silica sand). Table 6 shows the values of the leaching test compared to the limits recommended by Decreto 3 agosto 2005 of the Italian government for inert wastes. As it can be seen, the major success of this approach is the suppression of the leaching of toxic heavy metals; for example, Hg was not released at all from the vitrified products while a non-negligible release occurred from the as-such fly ashes. The detected Cd is also well below the limit identifying inert materials. Other heavy metals such as Ni, Pb, and Cr are less toxic, and their limit value is therefore higher. Overall, these results show the success of this approach in making the hazardous ashes safe.

Table 6. Leaching test before and after vitrification. ND stands for Not Detected. The limits are shown for inert waste according to "Decreto 3 agosto 2005" Of Italian government.

Elements (ppb)	Before Vitrification				After Vitrification				Limit
	FA1	FA2	Glass cullet	Silica Sand	G1	G2	G3	G4	
Hg	23.08	16.64	ND	ND	ND	ND	ND	ND	1.00
Cd	ND	ND	0.01	0.03	0.04	0.01	0.00	0.02	4.00
Ni	1.39	1.13	0.16	0.11	0.30	0.93	0.08	0.23	40.00
Pb	ND	ND	0.05	0.08	0.06	0.01	0.05	0.64	50.00
Cr	15.00	14.42	ND	ND	ND	0.50	ND	ND	50.00

*ND: No Detection; below the detection limit

4. Conclusions

In this work, fly ash from two different municipal solid waste incinerators were analyzed and vitrified. The vitrification is aimed to safely encapsulate the heavy metals within the glass composition. Fly ash samples were vitrified with the addition of 50 wt% silica sand and glass cullet at 1450°C and 1300°C, respectively. These additives were selected due to their easy availability and low cost, which are key features in an industrial scenario. The XRD analysis of vitrified ashes confirmed the success of the prepared batches.

The main difficulty associated with fly ash vitrification arises from their chemical composition variation in different incinerators, making the reported data very scattered and non-formulated. We have compared the composition of our successfully vitrified batches to some previously reported vitrified samples in the SiO_2-Al_2O_3-CaO, and SiO_2-ΣM_2O_3-$\Sigma(MO+M_2O)$ ternary phase diagrams, identifying a region where most data are reported. The normalized values for their composition in a SiO_2-Al_2O_3-CaO system show that most of them have the CaO/SiO_2 (C/S) ratio of about 0.44. Considering the effect of all major oxides

in the vitrification batches reported in literature, ternary diagram of SiO_2-ΣM_2O_3-$\Sigma(MO+M_2O)$ shows similar trends to the SiO_2-Al_2O_3-CaO ternary phase diagram. The degree of polymerization (Q) in the batches was calculated to be around 3.45 for 75% of reported data. This is an important finding bringing us one step closer to formulate the fly ash vitrification batches.

Finally, the standard leaching test was carried out on the fly ash samples before and after vitrification and showed the elimination of Hg leaching, as well as decreasing the rest of heavy metal leaching significantly below the limiting values for inert wastes, demonstrating the feasibility of this process for a circular economy approach.

5. Acknowledgments

6. References

[1]   Kawai K, Tasaki T. Revisiting estimates of municipal solid waste generation per capita and their reliability. J Mater Cycles Waste Manag 2016. https://doi.org/10.1007/s10163-015-0355-1.

[2]   Ji L, Lu S, Yang J, Du C, Chen Z, Buekens A, et al. Municipal solid waste incineration in China and the issue of acidification: A review. Waste Manag Res 2016. https://doi.org/10.1177/0734242X16633776.

[3]   Perrot JF, Subiantoro A. Municipal waste management strategy review and waste-to-energy potentials in New Zealand. Sustain 2018. https://doi.org/10.3390/su10093114.

[4]   Luo H, Cheng Y, He D, Yang E-H. Review of leaching behavior of municipal solid waste incineration (MSWI) ash. Sci Total Environ 2019;668:90–103. https://doi.org/10.1016/J.SCITOTENV.2019.03.004.

[5]   Luna Galiano Y, Fernández Pereira C, Vale J. Stabilization/solidification of a municipal solid waste incineration residue using fly ash-based geopolymers. J Hazard Mater 2011. https://doi.org/10.1016/j.jhazmat.2010.08.127.

[6]   Aubert JE, Husson B, Sarramone N. Utilization of municipal solid waste incineration (MSWI) fly ash in blended cement: Part 2. Mechanical strength of mortars and environmental impact. J Hazard Mater 2007;146:12–9. https://doi.org/10.1016/J.JHAZMAT.2006.11.044.

[7]   Wong G, Fan X, Gan M, Ji Z, Ye H, Zhou Z, et al. Resource utilization of municipal solid waste incineration fly ash in iron ore sintering process: A novel thermal treatment. J Clean Prod 2020. https://doi.org/10.1016/j.jclepro.2020.121400.

[8]   Kinto K. Ash melting system and reuse of products by ARC processing. Waste Manag 1996.

https://doi.org/10.1016/S0956-053X(96)00088-8.

[9] Chen X, Bi Y, Zhang H, Wang J. Chlorides Removal and Control through Water-washing Process on MSWI Fly Ash. Procedia Environ Sci 2016. https://doi.org/10.1016/j.proenv.2016.02.086.

[10] Dontriros S, Likitlersuang S, Janjaroen D. Mechanisms of chloride and sulfate removal from municipal-solid-waste-incineration fly ash (MSWI FA): Effect of acid-base solutions. Waste Manag 2020;101:44–53. https://doi.org/10.1016/j.wasman.2019.09.033.

[11] Kim M, Kim HG, Kim S, Yoon JH, Sung JY, Jin JS, et al. Leaching behaviors and mechanisms of vitrified forms for the low-level radioactive solid wastes. J Hazard Mater 2020. https://doi.org/10.1016/j.jhazmat.2019.121296.

[12] Ojovan MI, Lee WE. Immobilisation of Radioactive Wastes in Glass. An Introd. to Nucl. Waste Immobil., 2005. https://doi.org/10.1016/b978-008044462-8/50019-3.

[13] Sharifikolouei E, Canonico F, Salvo M, Baino F, Ferraris M. Vitrified and nonvitrified municipal solid wastes as ordinary Portland cement (OPC) and sand substitution in mortars. Int J Appl Ceram Technol 2020;17. https://doi.org/10.1111/ijac.13447.

[14] Bassani M, Santagata E, Baglieri O, Ferraris M, Salvo M, Ventrella A. Use of vitrified bottom ashes of municipal solid waste incinerators in bituminous mixtures in substitution of natural sands. Adv Appl Ceram 2009;108:33–43. https://doi.org/10.1179/174367608X364285.

[15] Bernardo E, Scarinci G, Edme E, Michon U, Planty N. Fast-sintered gehlenite glass-ceramics from plasma-vitrified municipal solid waste incinerator fly ashes. J Am Ceram Soc 2009;92:528–30. https://doi.org/10.1111/j.1551-2916.2008.02892.x.

[16] Wang Q, Yan J-H, Chi Y, Li X-D, Lu S-Y. Application of thermal plasma to vitrify fly ash from municipal solid waste incinerators. Chemosphere 2010;78:626–30. https://doi.org/10.1016/j.chemosphere.2009.10.035.

[17] Károly Z, Mohai I, Tóth M, Wéber F, Szépvölgyi J. Production of glass-ceramics from fly ash using arc plasma. J Eur Ceram Soc 2007;27:1721–5. https://doi.org/10.1016/j.jeurceramsoc.2006.05.015.

[18] Alhadj-Mallah MM, Huang Q, Cai X, Chi Y, Yan JH. Vitrification of municipal solid waste incineration fly ash using biomass ash as additives. Environ Technol (United Kingdom) 2015;36:654–60. https://doi.org/10.1080/09593330.2014.957245.

[19] Vu DH, Wang K-S, Chen J-H, Nam BX, Bac BH. Glass–ceramic from mixtures of bottom ash and fly ash. Waste Manag 2012;32:2306–14. https://doi.org/10.1016/J.WASMAN.2012.05.040.

[20] Huang Q, Cai X, Alhadj-Mallah MM, Du C, Chi Y, Yan J. Thermal plasma vitrification of MSWI fly ash mixed with different biomass ashes. IEEE Trans Plasma Sci 2014;42:3549–54. https://doi.org/10.1109/TPS.2014.2358626.

[21] Park YJ, Heo J. Vitrification of fly ash from municipal solid waste incinerator. J Hazard Mater 2002;91:83–93. https://doi.org/10.1016/S0304-3894(01)00362-4.

[22] Gao J, Dong C, Zhao Y, Hu X, Qin W, Wang X, et al. Vitrification of municipal solid waste incineration fly ash with B2O3 as a fluxing agent. Waste Manag 2020;102:932–8. https://doi.org/10.1016/j.wasman.2019.12.012.

[23] National Center for Biotechnology Information. Sodium chloride, CID=5234. Pubchem Database 2020.

[24] Maeda K, Yasumori A. Toughening of CaO–Al2O3–SiO2 glass by dmisteinbergite precipitation. Mater Lett 2016. https://doi.org/10.1016/j.matlet.2016.05.123.

[25] Hemmings RT, Berry EE. On the Glass in Coal Fly Ashes: Recent Advances. MRS Proc 1987. https://doi.org/10.1557/proc-113-3.

[26] Henderson GS, Calas G, Stebbins JF. The Structure of Silicate Glasses and Melts. Elements 2006;2:269–73. https://doi.org/10.2113/gselements.2.5.269.

[27] Heo JH, Cho JW, Park HS, Park JH. Crystallization and vitrification behavior of CaO-SiO 2 -Fe t O-Al 2 O 3 slag: Fundamentals to use mineral wastes in production of glass ball. J Clean Prod 2019. https://doi.org/10.1016/j.jclepro.2019.04.035.

[28] Kucharczyk S, Sitarz M, Zajac M, Deja J. The effect of CaO/SiO2 molar ratio of CaO-Al2O3-SiO2 glasses on their structure and reactivity in alkali activated system. Spectrochim Acta Part A Mol Biomol Spectrosc 2018;194:163–71. https://doi.org/https://doi.org/10.1016/j.saa.2018.01.018.

[29] Mills KC, Karagadde S, Lee PD, Yuan L, Shahbazian F. Calculation of physical properties for use in models of continuous casting process-Part 1: Mould slags. ISIJ Int 2016. https://doi.org/10.2355/isijinternational.ISIJINT-2015-364.

[30] Mills KC, Yuan L, Li Z, Chou K-C, Zhang G. The factors affecting the thermophysical properties of slags and glasses. CDROM, Molten 2012.

[31] Haugsten KE, Gustavson B. Environmental properties of vitrified fly ash from hazardous and municipal waste incineration. Waste Manag 2000. https://doi.org/10.1016/S0956-053X(99)00325-6.

[32] Yang Y, Xiao Y, Voncken JHL, Wilson N. Thermal treatment and vitrification of boiler ash from

a municipal solid waste incinerator. J Hazard Mater 2008;154:871–9.

https://doi.org/10.1016/J.JHAZMAT.2007.10.116.

[33]   Tian S, Li J, Liu F, Guan J, Dong L, Wang Q. Behavior of Heavy Metals in the Vitrification of

MSWI Fly Ash with a Pilot-scale Diesel Oil Furnace. Procedia Environ Sci 2012;16:214–21.

https://doi.org/10.1016/j.proenv.2012.10.030.

[34]   Tsakalou C, Papamarkou S, Tsakiridis PE, Bartzas G, Tsakalakis K. Characterization and

leachability evaluation of medical wastes incineration fly and bottom ashes and their vitrification

outgrowths. J Environ Chem Eng 2018;6:367–76. https://doi.org/10.1016/j.jece.2017.12.012.

[35]   Čarnogurská M, Lázár M, Puškár M, Lengyelová M, Václav J, Širillová ˏubomíra. Measurement

and evaluation of properties of MSW fly ash treated by plasma. Meas J Int Meas Confed

2015;62:155–61. https://doi.org/10.1016/j.measurement.2014.11.014.

[36]   Wang Q, Tian S, Wang Q, Huang Q, Yang J. Melting characteristics during the vitrification of

MSWI fly ash with a pilot-scale diesel oil furnace. J Hazard Mater 2008;160:376–81.

https://doi.org/10.1016/j.jhazmat.2008.03.043.

[37]   Peng F, Liang K, Hu A, Shao H. Nano-crystal glass-ceramics obtained by crystallization of

vitrified coal fly ash. Fuel, 2004. https://doi.org/10.1016/j.fuel.2004.04.008.

[38]   Ito T. Vitrification of fly ash by swirling-flow furnace. Waste Manag 1996.

https://doi.org/10.1016/S0956-053X(96)00090-6.

[39]   Ni G, Zhao P, Jiang Y, Meng Y. Vitrification of MSWI fly ash by thermal plasma melting and

fate of heavy metals. Plasma Sci Technol 2012. https://doi.org/10.1088/1009-0630/14/9/08.